Journal of Molecular Catalysis A: Chemical 310 (2009) 150–158

Contents lists available at ScienceDirect

Journal of Molecular Catalysis A: Chemical

journal homepage: www.elsevier.com/locate/molcata

Acetalization of glycerol using mesoporous MoO_3/SiO_2 solid acid catalyst

Shubhangi B. Umbarkar[a], Trupti V. Kotbagi[a], Ankush V. Biradar[a], Renu Pasricha[b], Jyoti Chanale[a], Mohan K. Dongare[a,*], Anne-Sophie Mamede[c], Christine Lancelot[c], Edmond Payen[c]

[a] Catalysis Division, National Chemical Laboratory, Dr. Homi Bhabha Road, Pune, Maharashtra 411008, India
[b] Centre for Material Characterization, National Chemical Laboratory, Dr. Homi Bhabha Road, Pune, Maharashtra 411008, India
[c] Unité de Catalyse et de Chimie du Solide, UMR CNRS 8181, USTL, France

ARTICLE INFO

Article history:
Received 26 January 2009
Received in revised form 4 June 2009
Accepted 6 June 2009
Available online 16 June 2009

Keywords:
Acetalization
Solid acid
Glycerol
Aldehyde
Silicomolybdic acid

ABSTRACT

Acetalization of glycerol with various aldehydes has been carried out using mesoporous MoO_3/SiO_2 as a solid acid catalyst. A series of MoO_3/SiO_2 catalysts with varying MoO_3 loadings (1–20 mol%) were prepared by sol–gel technique using ethyl silicate-40 and ammonium heptamolybdate as silica and molybdenum source respectively. The sol–gel derived samples were calcined at 500 °C and characterized using various physicochemical characterization techniques. The XRD of the calcined samples showed the formation of amorphous phase up to 10 mol% MoO_3 loading and at higher loading of crystalline α-MoO_3 on amorphous silica support. TEM analyses of the materials showed the uniform distribution of MoO_3 nanoparticles on amorphous silica support. Raman spectroscopy showed the formation of silicomolybdic acid at low Mo loading and a mixture of α-MoO_3 and polymolybdate species at high Mo loadings. Moreover the Raman spectra of intermediate loading samples also suggest the presence of β-MoO_3. Acetalization of glycerol with benzaldehyde was carried out using series of MoO_3/SiO_2 catalysts with varying MoO_3 loadings (1–20 mol%). Among the series, MoO_3/SiO_2 with 20 mol% MoO_3 loadings was found to be the most active catalyst in acetalization under mild conditions. Maximum conversion of benzaldehyde (72%) was obtained in 8 h at 100 °C with 60% selectivity for the six-membered acetal using 20% MoO_3/SiO_2. Interestingly with substituted benzaldehydes under same reaction conditions the conversion of aldehydes decreased with increase in selectivity for six-membered acetals. These results indicate the potential of this catalyst for the acetalization of glycerol for an environmentally benign process.

1. Introduction

Glycerol is a 10% by-product of biodiesel production leading to an alarming increase of crude glycerol in the market with currently 350,000 tons per annum (tpa) production in the USA and 600,000 tpa in Europe which will still increase due to replacement of 5.75% of petroleum fuels with biofuel by 2010 [1]. Synthesis of value-added molecules from crude glycerol is an attractive alternative to disposal by incineration. Some potential uses for glycerol include: hydrogen gas production [2], glycerine acetate as a potential fuel additive [3], composite additive, citric acid production, cosmetic bonding agent for makeup including eye drops and conversion to propylene glycol [4], acrolein [5,6], ethanol [7] and epichlorhydrin [8,9]. Glycerol may be used as antifreeze agent [10]. One more application of glycerol is the acetalization with aldehydes and ketones to [1,3] dioxan-5-ol (isomeric six- and five-membered cyclic acetals as novel fine intermediates. Six-membered cyclic acetals are potential precursors for the production of green platform chemicals 1,3-dihydroxyacetone and 1,3-propanediol [11]. The acetalization reaction is many times necessary for protection of carbonyl groups during the manipulation of multifunctional organic molecules [12] as well as it has direct applications as fragrances, in cosmetics, food and beverage additives, pharmaceuticals, in detergents, in lacquer industries and as ignition accelerators and antiknock additives in combustion engines [13–16] and in port wine production [17]. Glycerol acetals can also be used as the basis for surfactants [18]. In the acetalization reaction usually 50% of each five- and six-membered acetals are obtained. Efforts have been taken to change and control this ratio by varying the reaction parameters such as temperature, aldehyde or ketone to glycerol ratio and the choice of solvent. The general method for acetal synthesis is reaction of carbonyl compounds with an alcohol or an orthoester in the presence of acid catalysts. The commercial catalysts used are strong acids such as PTSA, HCl, H_3PO_4, and divinylbenzene–styrene resin [19]. A number of acetalization procedures include the use of protic acids, Lewis acids (zinc chloride) [20], alumina [21], montmorillonite [22,23], zeolites [24–27], mesoporous aluminosilicates [28,29] and ion exchange resins [19,30]. Acetalization of aldehydes can be performed in the presence of weak acids, while ketones need

* Corresponding author. Tel.: +91 20 25902044; fax: +91 20 25903761.
E-mail address: mk.dongare@ncl.res.in (M.K. Dongare).

1381-1169/$ – see front matter © 2009 Elsevier B.V. All rights reserved.
doi:10.1016/j.molcata.2009.06.010

stronger acids like sulfuric, hydrochloric or *p*-toluenesulfonic acid and larger amounts of catalyst. However methods mentioned above present limitations such as use of expensive reagents, tedious work-up procedure and necessity of neutralization of the strongly acidic media leading to production of undesired wastes. In this sense synthetic zeolites appear to be promising catalysts with the obvious advantages over conventional Brønsted or Lewis acids [31,32] of easy separation from the reaction mixture, shape selectivity, and reusability. Supported metal oxides are well known for catalyzing a large variety of reactions. Thus many studies have been devoted to the preparation and characterization of these solids. Molybdenum oxide catalysts supported on SiO_2, Al_2O_3 and TiO_2 have been extensively investigated because of their catalytic activity in oxidation and acid catalyzed organic reactions [33–37].

We have successfully established the synthesis of mesoporous MoO_3/SiO_2 solid acid catalyst by sol–gel technique using ethyl silicate-40 as novel silica source without using any surfactant template and the catalyst has been found to be very active for acid catalyzed organic reactions such as nitration of benzene and cumene [38,39], transesterification of diethyl oxalate to diphenyl oxalate [37] and Beckmann rearrangement [40]. In continuation of our efforts to explore wider applicability of these MoO_3/SiO_2 catalysts for acid catalyzed organic transformations, detailed catalyst characterization using HR-TEM and Raman spectroscopy as well as acetalization of glycerol with various aldehydes has been carried out. Based on the characterization results the catalyst activity has been correlated with the structural features of the catalyst and the results are reported in this paper.

2. Experimental

2.1. Materials

All the reagents viz., ammonium heptamolybdate (AHM), ethyl silicate-40, isopropyl alcohol, glycerol, aldehydes, toluene were of AR grade (99.8%) and were obtained from S.D. Fine, LOBA and Merck chemicals, India. The chemicals were used without further purification.

2.2. Catalyst preparation

MoO_3/SiO_2 catalysts with varying molybdenum oxide molar concentrations (1, 5, 10, 15, 20) were prepared. AHM and ethyl silicate-40 (CAS registry no. 18945-71-7) were used as molybdenum and silica sources, respectively. In a typical procedure 20 mol% MoO_3/SiO_2 catalyst was synthesized by dissolving 14.11 g AHM in 40 ml water at 80 °C. This hot solution was added drop wise to the dry isopropyl alcohol solution of ethyl silicate-40 (48.0 g) with constant stirring. The resultant transparent greenish gel was air dried and calcined at 500 °C in air in a muffle furnace for 12 h. Similarly catalysts with 1, 5, 10, 15 mol% molybdenum oxide loadings were prepared.

Pure high surface area silica catalyst was prepared for comparison by adding 52 g ethyl silicate-40 to 30 g dry isopropyl alcohol; to this mixture 0.02 g ammonia solution (25%) was slowly added with constant stirring. The transparent white gel thus obtained was air dried and calcined in a muffle furnace at 500 °C for 12 h.

2.3. Catalyst characterization

The X-ray diffraction analysis was carried out using Rigaku X-ray diffractometer (Model DMAX IIIVC) with Cu Kα (1.542 Å) radiation. Temperature programmed desorption of ammonia (TPD-NH_3) was carried out using Micromeritics Autocue 2910. BET surface area was determined using NOVA 1200 Quanta chrome.

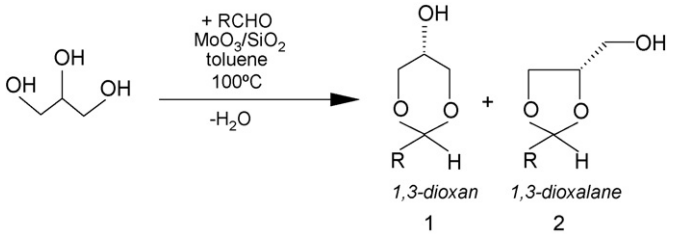

Scheme 1. Acetalization of glycerol with aldehydes.

Acidity of the samples was determined by pyridine adsorption studies using Shimadzu 8000 series FTIR spectrometer using DRIFT technique. The sample was placed in the DRIFT cell and heated to 400 °C in flow of inert gas (N_2) for 2 h. It was cooled to 100 °C and pyridine was adsorbed on the sample in N_2 flow. The physisorbed pyridine was removed by flushing the cell with N_2 for 45 min at the same temperature and the spectrum was recorded. Then pyridine was desorbed for 45 min at 200, 300 and 400 °C and spectra were recorded at each temperature. The spectrum of the neat catalyst (before pyridine adsorption) at 100 °C was subtracted from all the spectra.

TEM measurements were performed on a JEOL model 1200EX instrument operating at an accelerating voltage at 120 kV and on a Tecnai G2-20 FEI instrument operating at an accelerating voltage at 200 kV. Before analysis, the powders were ultrasonically dispersed in ethanol, and two drops of ethanol containing the solid were deposited on a carbon coated copper grid.

Raman spectra were recorded under ambient conditions on a LabRAM infinity spectrometer (Horiba–Jobin–Yvon) equipped with a liquid nitrogen detector and a frequency doubled Nd-YAG laser supplying the excitation line at 532 nm with 1–10 mW power. The spectrometer is calibrated using the Si line at 521 cm^{-1} with a spectral resolution of 3 cm^{-1}.

2.4. Typical reaction procedure

A typical acetalization reaction of glycerol with aldehydes (Scheme 1) was carried out in a 50-ml two-necked round bottom flask fitted with a dean-stark apparatus. The flask was charged with glycerol (0.11 mol), aldehyde (0.1 mol), catalyst (10% of glycerol) and solvent (15 g). The reaction mixture was vigorously stirred at 100 °C and reaction was continued till maximum conversion. Reaction was monitored by GC. Samples were withdrawn at regular time intervals and analyzed using a Hewlett-Packard GC model HP6890 with HP-5 (5% cross-linked polyethylene siloxane) column (diameter: 0.53 mm, film thickness: 1 μm, length: 60 m). After completion of the reaction, reaction mixture was cooled and filtered. The products were confirmed by GC-MS (model GC Agilent 6890N with HP-5 and MS Agilent 5973 network MSD, fitted with 30 m capillary column and GC-IR model PerkinElmer spectrum 2001, column DB-5 and 25-m length 0.32 mm internal diameter).

3. Results and discussion

3.1. XRD characterizations

The XRD patterns of all the catalysts prepared by sol–gel are shown in Fig. 1. For comparison, the XRD pattern of pure silica is also included (Fig. 1a). The patterns show the amorphous nature of the material at low Mo loadings (Fig. 1b–d) indicating a very high dispersion of amorphous molybdenum oxo species on amorphous silica support up to 10 mol% loading of molybdenum oxide. The XRD patterns of the 15 and 20% Mo loaded catalysts (Fig. 1e and f) exhibit sharp peaks on the broad underlying peaks characteristic

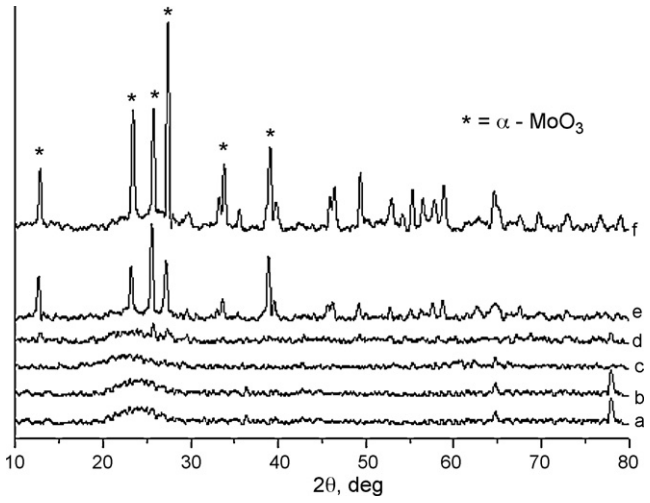

Fig. 1. XRD of silica (a) and sol–gel MoO_3/SiO_2 with 1% (b), 5% (c), 10% (d), 15% (e), and 20% (f) MoO_3.

of the amorphous silica at $2\theta = 24^\circ$. These intense peaks observed at $2\theta = 12.9$, 23.4, 25.8 and 27.4° are characteristic of the α-MoO_3 orthorhombic phase [41]. It is interesting to note that even though the MoO_3 is in the crystalline form at higher Mo loading, the silica support still retains its amorphous nature leading to the high surface area of the catalysts [36]. It appears from the XRD results that up to 10 mol% MoO_3 loading there is a uniform dispersion of amorphous molybdenum oxo species on silica support, however at higher loading; MoO_3 crystalline bulk phase is formed on amorphous silica support.

3.2. Textural characterization

The surface areas of all the catalysts were determined using the BET method [36]. The detailed textural characterization and acidity measurements of all the catalysts are summarised in Table 1. The mesoporosity of the catalysts was evident for all the catalysts including silica (Fig. 2). No specific trend can be deduced with increase in the Mo loading. It is interesting to note that even though no organic template is used during the synthesis of pure silica as well as MoO_3/SiO_2, the product formed shows a mesoporous nature. Thus the pore size is in the range of 40 Å for the samples containing 1–10 mol% MoO_3. At higher Mo loading the pores diameter is not uniform, which can be due to the uncontrolled hydrolysis of ETS-40. Hence no specific trend could be observed for pore size of 1–20% MoO_3/SiO_2, attributed to absence of template during synthesis as well as no control on the amount of water added for hydrolysis due to varying amount of water needed for dissolution of AHM. Use of ethyl silicate-40 as silica source led to very high surface area material (606 m^2/g). This is a polymeric form (trimeric and tetrameric) of tetraethyl orthosilicate monomer that upon controlled hydrolysis yields very high specific surface area silica. Indeed the trimeric and tetrameric silicon ethoxide structures after hydrolysis restrict the growth of large particles resulting in mesoporous high surface area silica. The surface area was found to decrease when increasing the MoO_3 loading from 1 to 20 mol%, however no direct trend can be deduced because of uncontrolled rate of hydrolysis with increase in the Mo loading due to the amount of water needed to dissolve AHM at higher MoO_3 loading cannot be controlled. This affects the nature of the resulting gel.

3.3. Vibrational spectroscopic study

Raman spectroscopic analysis after calcination and transfer in air allowed us to have a better insight in the exact nature of the deposited oxomolybdenum species. The Raman spectra of the calcined samples prepared by sol–gel method at low (1 and 5%) and high (10, 15 and 20%) loadings are, respectively, shown in Figs. 3 and 4.

The broad line at 450–500 cm^{-1}, centered at 480 cm^{-1} (Fig. 3a) is due to the silica support. The two low Mo loading samples exhibit the same Raman lines at 247, 629, 961 and 981 cm^{-1} that are assigned to the silicomolybdic heteropolyanion (HPA) $[SiMo_{12}O_{40}]^{4-}$ (SMA) inside silica pores [42]. As the Mo loading increases, new Raman lines appear at 213, 383 and 876 cm^{-1}, the exact origin of which is not clearly established. However they are not observed at high Mo loading. At higher Mo loading, from 10 to 20% MoO_3, the Raman spectra exhibit the lines characteristic of α-MoO_3 (161, 285, 293, 339, 381, 666, 819 and 996 cm^{-1}) [43]. However in the 10% MoO_3/SiO_2 spectrum (Fig. 4c), the above mentioned features of the SMA (981, 666 and 247 cm^{-1}) are still observed together with lines at 952 and 889 cm^{-1} characteristic of a well dispersed polymolybdate species by reference to literature [44]. In the Raman spectra of the 15 and 20% MoO_3/SiO_2, these features are no longer observed [45]. However, a weak line is observed at 960 cm^{-1} in Fig. 5e that could also correspond to a surface polymolybdate species. In the spectrum of 15% MoO_3/SiO_2 (Fig. 4d) two new lines are observed at 852 and 778 cm^{-1} that are assigned to the formation of β-MoO_3 [46,47].

The nature of the molybdenum species formed versus the Mo loading is in agreement with the evolution of the Raman spectra of the dried solids that are shown in Fig. 5. At low Mo loading (typically 1 and 5%) they exhibit a broad line at 960 cm^{-1} that is characteristic of a well dispersed polymolybdate phase. A shoulder is observed at 980 cm^{-1} on its high wavenumber side that, together with the line at 626 and 248 cm^{-1}, is characteristic of the molecular silicomolybdic entities, the amount of which being very low. At higher Mo loading, the spectra (Fig. 5c–e) exhibit the main lines characteristic of the AHM that transforms into α MoO_3 upon calcination.

Up to 10% Mo loading presence of silicomolybdic acid as well as well dispersed polymolybdate phase was observed in the Raman spectra of the samples after calcination and transfer in air. It is well documented that hydration occurs in air [48,49] after the calcination and it can be considered that a thin film of water covers the silica surface, which is also suggested for Mo/SiO_2 prepared by impregnation [50]. The presence of SMA at low Mo loading is directly correlated to the ZPC (zero point of charge) of such silica support, which allows preservation of this HPA, which is only sta-

Table 1
Surface area and acidity of the MoO_3/SiO_2 catalysts.

Catalyst	Surface area, m^2/g	Pore volume, cm^3/g	Average pore diameter, Å	NH_3 desorbed, mmol/g
Silica	606	0.61	70.49	0.03
1% MoO_3/SiO_2	583	0.59	40.69	0.18
5% MoO_3/SiO_2	432	0.63	58.20	0.56
10% MoO_3/SiO_2	284	0.57	79.60	0.71
15% MoO_3/SiO_2	275	0.51	74.20	0.86
20% MoO_3/SiO_2	180	0.23	71.64	0.94

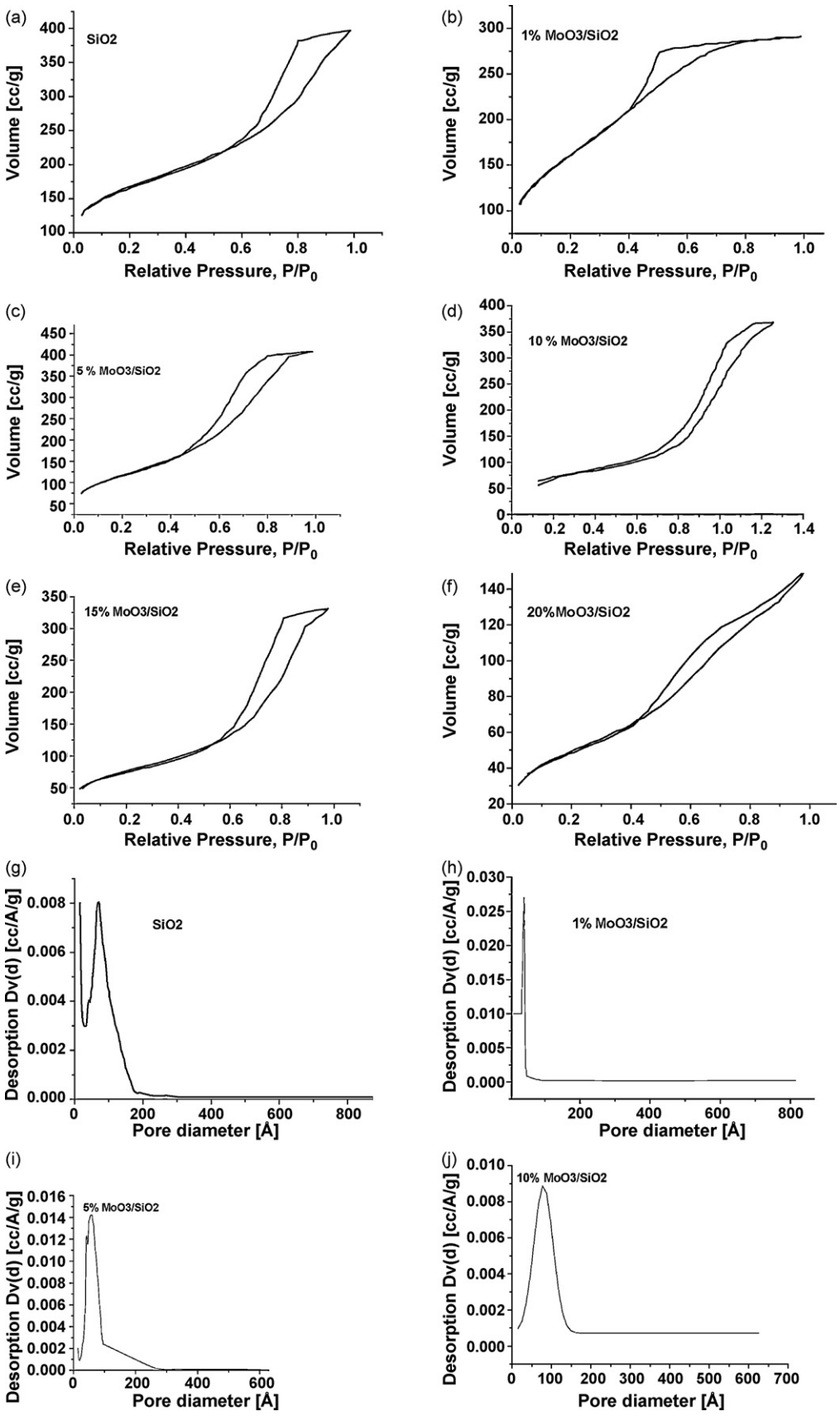

Fig. 2. Adsorption desorption isotherm of silica (a) and sol–gel MoO_3/SiO_2 with 1% (b), 5% (c), 10% (d), 15% (e), and 20% (f) MoO_3 and pore size distribution of silica (g) and MoO_3/SiO_2 with 1% (h), 5% (i), 10% (j), 15% (k), and 20% (l) MoO_3 loading.

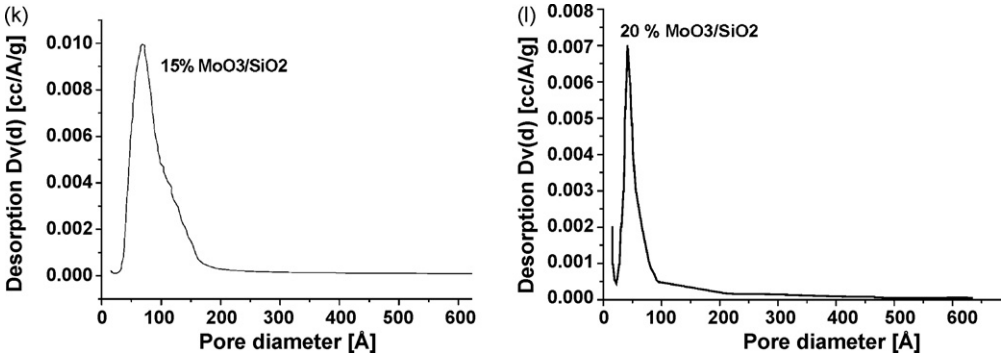

Fig. 2. (*Continued*).

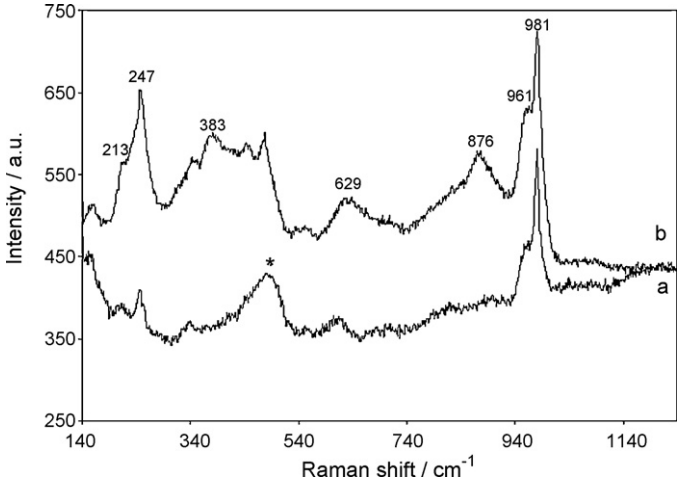

Fig. 3. Raman spectra of (a) 1% MoO_3 and (b) 5% MoO_3 supported on silica prepared by sol–gel method and calcined at 500 °C.

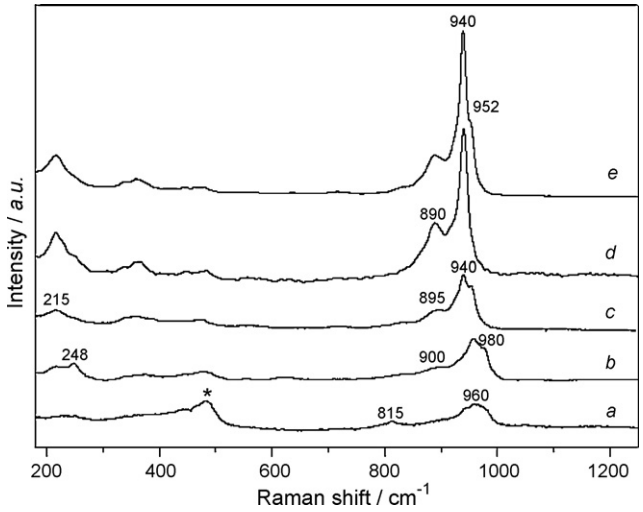

Fig. 5. Raman spectra of (a) 1% MoO_3, (b) 5% MoO_3, (c) 10% MoO_3, (d) 15% MoO_3 and (e) 20% MoO_3 supported on silica prepared by sol–gel method and then dried at 100 °C.

ble in solution at low pH values typically below 2. The increase in the Mo loading leads to an increase in the pH of the solution inside the pores, which induces the presence of a well dispersed surface polymolybdate. This explains why SMA is mainly observed at low loading in the calcined solids whereas it is not observed before calcination, due to the pH of the dried gel (pH 7). The formation of this SMA heteropolyanion is not observed in the dried sample, which could be assigned to the fact that the SiO_2 is not formed in dried sample and the ZPC of the amorphous gel is higher than that of the above mentioned pH stability limit. At 10% MoO_3 the β-MoO_3 is evidenced by Raman spectroscopy. However the β-MoO_3 phase was not detected by the XRD technique. It should be present as microcrystallites well dispersed inside the silica framework (not observed by XRD). Thus this preparation method allowed us to

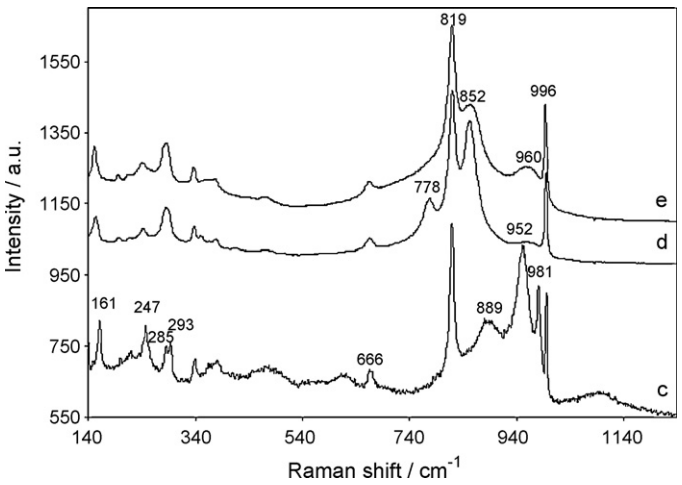

Fig. 4. Raman spectra of (c) 10% MoO_3, (d) 15% MoO_3 and (e) 20% MoO_3 supported on silica prepared by sol–gel method and then calcined at 500 °C.

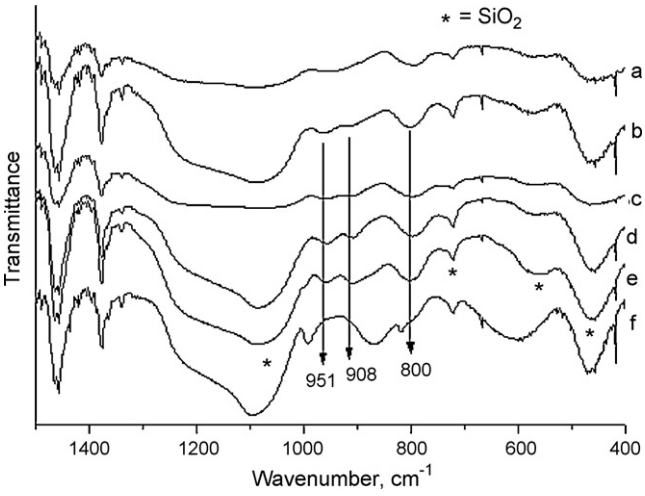

Fig. 6. FTIR spectra of silica (a) and MoO_3/SiO_2 with 1% (b), 5% (c), 10% (d), 15% (e), and 20% (f) MoO_3 loading by sol–gel technique.

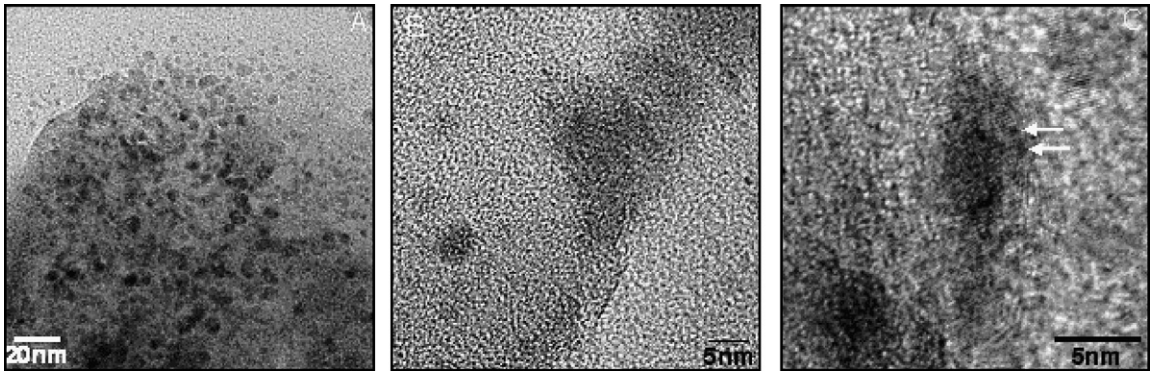

Fig. 7. TEM micrograph of 1% MoO_3/SiO_2 prepared by sol–gel at different magnification and focused on different area.

stabilize this phase even after calcination at 500 °C, a temperature at which the transformation into its orthorhombic form should have been observed. At higher Mo loading (10, 15, 20%) the formation of α-MoO_3 is observed. However this formation can be correlated to the precipitation of ammonium heptamolybdate as evidenced by the Raman spectroscopic study of the dried solids. This would lead to a lower interaction between the molybdenum oxo species and the silica and consequently to the formation of α-MoO_3 as in the classical impregnation. This suggests that the β-MoO_3 phase could originate from the well dispersed oxomolybdate phase, and its stabilization is induced by the interaction with the support.

The FTIR spectra of all the catalyst samples prepared by sol–gel technique presented in Fig. 6 also confirm the formation of the α-MoO_3 at higher loading (main bands at 993, 872, and 570 cm^{-1}) whereas the spectra of the 1–5 mol% loading (Fig. 6b–e) show mainly the bands of the silica with those of oxo molybdenum species (908 and 951 cm^{-1}) [50].

3.4. TEM analysis

The existence of nanosized MoO_3 particles on the mesoporous silica support is corroborated by TEM analysis. Typical TEM micrographs of the calcined solids are reported in Figs. 7–11.

For the different Mo loadings (1–20 mol%), Figs. 7, 8, 9a, 10 and 11a show the presence of small MoO_3 particles dispersed on the silica support, with a size comprised between 1 and 2 nm.

The distribution of nano MoO_3 seems to be increasing with Mo loading as seen in the TEM images of the 20% MoO_3 sample: in Fig. 11B, areas with larger particles (6–8 nm) can be evidenced.

Together with these nanoparticles, bulk MoO_3 appears to be present in the samples with high Mo loadings (from 10 mol%), as shown in Fig. 10b and 11c. These particles are very large, their size being about the micron. These results are in good agreement with the Raman spectroscopic study showing the presence of bulk MoO_3 on the samples with 10, 15 and 20 mol% Mo loadings, possibly resulting from AHM precipitation as mentioned before. The quantity of this compound may not be sufficient to be detected by XRD in the 10% Mo sample.

The ammonia and pyridine adsorption is studied on the solids activated by a thermal treatment (preactivation at 450 °C). However this treatment modifies the nature of the well dispersed surface oxomolybdate species as it has been clearly shown by Raman spectroscopy [51]. The coordination of the Mo being lower than 6, pre-activated solids would exhibit Lewis acid site rather than Brønsted ones, which is in agreement with the pyridine acidity measurement. Thus the ammonia desorption at low temperature on these solids should correspond to ammonia molecules adsorbed on Lewis acid sites. Upon increasing the Mo loading this acidity is still observed in agreement with Raman spectroscopy as the lines characteristic of the aforementioned well dispersed oxomolybdate phase are still observed. Stronger acidity is evidenced by NH_3-TPD [36] at this high Mo loading whereas pyridine adsorption shows the existence of Brønsted sites also. It can be considered that the Brønsted acidity observed at higher Mo loading contributes to overall increase in the total acidity, which is seen by NH_3-TPD. Such evolution is in agreement with the Raman spectroscopic characterization, which proves the presence of the above mentioned surface oxomolybdate phase and of a mixture of α- and β-MoO_3

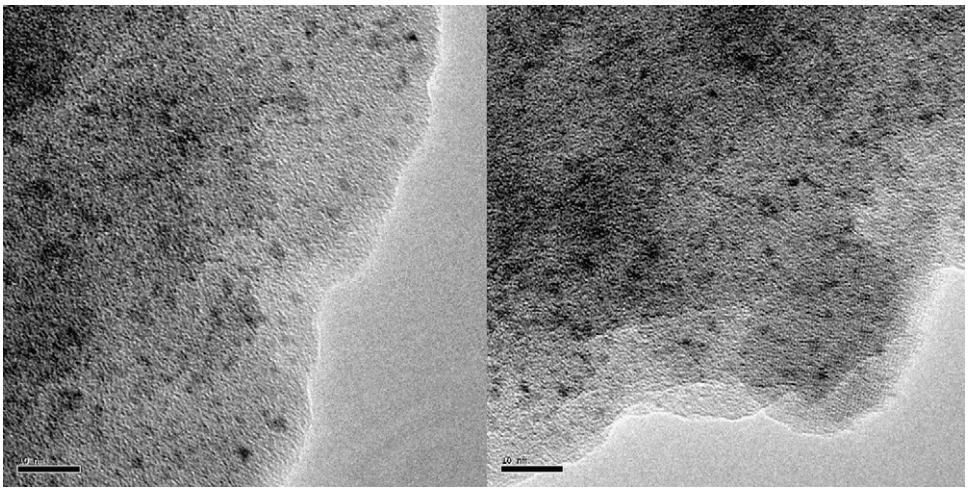

Fig. 8. TEM micrograph of 5% MoO_3/SiO_2 prepared by sol–gel focused on different area.

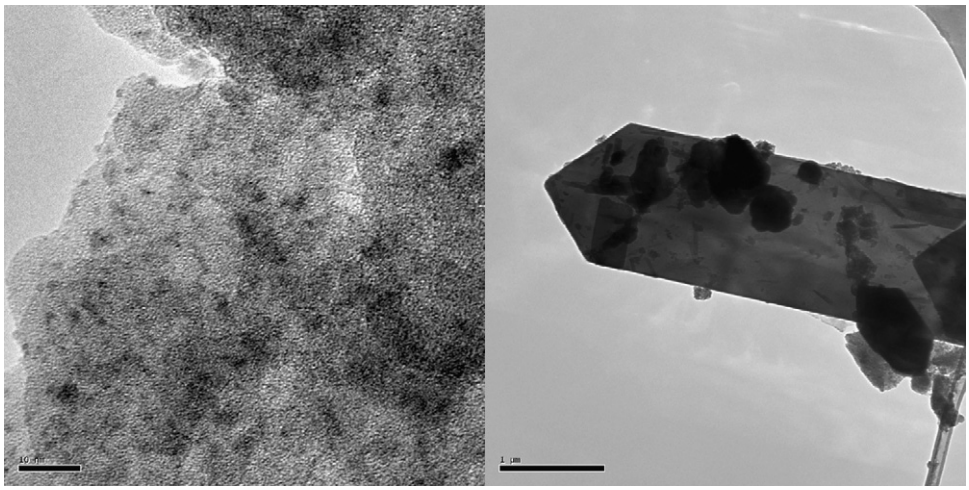

Fig. 9. TEM micrograph of 10% MoO_3/SiO_2 prepared by sol–gel focused on different area.

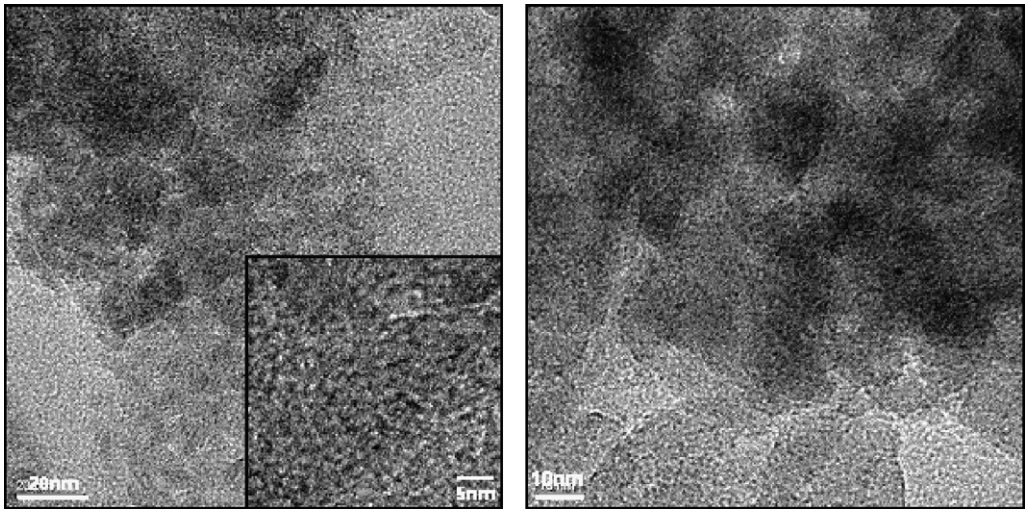

Fig. 10. TEM micrograph of 15% MoO_3/SiO_2 prepared by sol–gel at different magnification and focused on different area.

nanoparticles, their relative amount depending on the Mo loading. Both MoO_3 phases could be responsible for this new Brønsted acidity. This is in agreement with literature data showing that bulk MoO_3 may exhibit Brønsted acidity.

3.5. Catalytic activity

The reaction of glycerol with benzaldehyde as model substrate was studied initially. Acetalization of glycerol with benzaldehyde

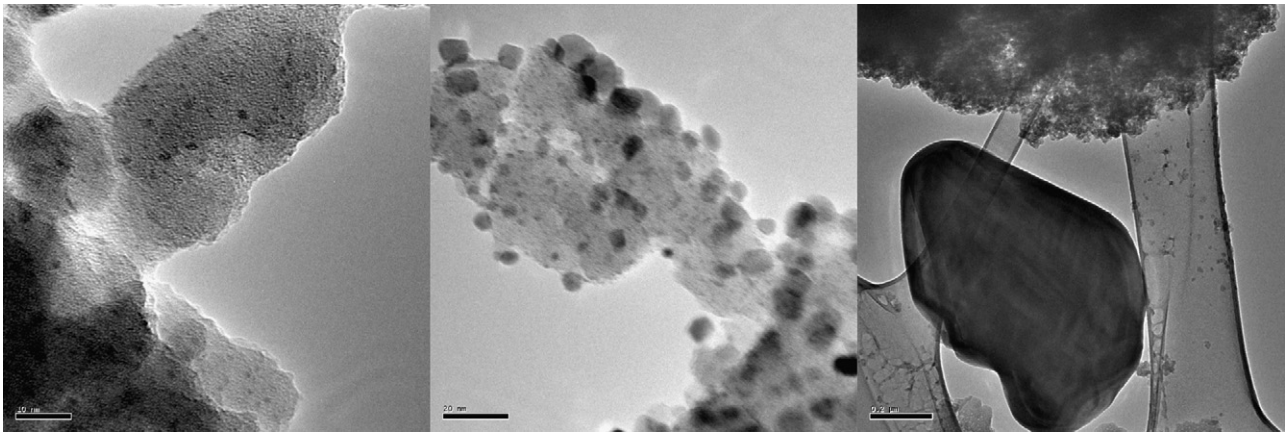

Fig. 11. TEM micrograph of 20% MoO_3/SiO_2 prepared by sol–gel focused on different area.

Table 2
Acetalization of glycerol with benzaldehyde using different loadings of MoO_3/SiO_2.

Sr. no.	Catalyst	Conversion, %	Selectivity, %	
			Six-membered	Five-membered
1.	Blank	20	49	51
2.	*p*-Toluene sulfonic acid[a]	81	63	37
3.	Pure SiO_2	23	50	50
4.	1% MoO_3/SiO_2	37	63	37
5.	10% MoO_3/SiO_2	43	62.5	37.5
6.	20% MoO_3/SiO_2	72	60	40

Charge: glycerol = 0.11 mol, benzaldehyde = 0.1 mol, catalyst = 10 wt% of glycerol, reaction temp = 100 °C, solvent = toluene 15 g, time = 8 h.
[a] Benzaldehyde: *p*-TSA = 500:1.

was carried out using series of MoO_3/SiO_2 catalysts with different MoO_3 molar loadings on silica and the results are given in Table 2. The results are also compared with blank reaction (without catalyst) (Table 2, entry 1), conventionally used *p*-toluene sulphonic acid (*p*-TSA) (Table 2, entry 2) and only silica as catalyst (Table 2, entry 3). Benzaldehyde conversion with 1 and 10% MoO_3 loading was 38% and 45% (Table 2, entry 4 and 5), respectively, which increased to 72% in presence of 20% MoO_3/SiO_2 (Table 2, entry 6). In all the cases selectivity for six-membered and five-membered acetals was 60% and 40%, respectively.

The results clearly show that activity increases with increase in the MoO_3 loading and the maximum catalytic activity was obtained with 20% MoO_3/SiO_2. The results of catalytic reaction were compared with blank reaction and a remarkable difference in conversion and selectivity was observed. The blank reaction afforded only 20% benzaldehyde conversion with 49% selectivity for the six-membered acetal (Table 2, entry 1). When pure silica was used as a catalyst for the reaction only 23% benzaldehyde conversion was obtained with 50% selectivity for the six-membered acetal (Table 2, entry 3). Whereas with conventional homogeneous *p*-TSA catalyst 81% benzaldehyde conversion was obtained with 63% selectivity for the six-membered acetal (Table 2, entry 2). When 20% MoO_3/SiO_2 was used as catalyst 72% benzaldehyde conversion with 60% selectivity for the six-membered acetal was obtained (Table 2, entry 6). The role of catalyst in this reaction is thus clearly evident. This suggests that nanosized molybdenum oxo species uniformly dispersed on mesoporous silica support imparting acidity are the active species for acetalization. As 20% MoO_3/SiO_2 showed maximum catalytic activity, acetalization of glycerol with various aldehydes was carried out using this catalyst.

The results of acetalization of glycerol with various aldehydes are shown in Table 3. Condensation of glycerol with benzaldehyde gave 72% conversion with 60% selectivity for six-membered acetal (Table 2, entry 6). It was observed that in case of substituted benzaldehydes electron donating or electron withdrawing substitution on phenyl ring led to decrease in glycerol conversion but with increase in selectivity for six-membered acetal. The drastic decrease in the conversion (23%) was observed in case of nitro and hydroxyl substitution at *meta*- and *ortho*-position, respectively (Table 3, entry 2). In case of chloro- or other electron withdrawing substitution the conversion did not decrease significantly (Table 3, entry 4). However in case of *trans*-cinnamaldehyde very low conversion of only 10% was obtained (Table 3, entry 7). This may be due to unsaturation leading to decrease in the electrophilic character of carbonyl carbon. Aliphatic aldehydes gave comparatively higher conversions compared to aromatic aldehydes.

Corma and co-workers [52] have reported acetalization of glycerol with phenyl acetaldehyde using various zeolites at higher temperature (~150 °C). USY-2 zeolite has shown up to 95% conversion and the selectivity for 1,3-dioxane/1,3-dioxolane 64/31 and in case of beta-2 and PTSA > 90% conversion was obtained. However with modernite and MCM-41 as well as ZSM-5 the conversion has decreased drastically up to 35% and 54%, respectively. In all the cases selectivity for five-membered acetal is slightly higher. When same zeolites were used for acetalization of propylene glycol with vanillin the yields in the range of 81–91% were obtained. In this work the glycerol or glycol is used in excess (2.5 equivalent). In the present work the selectivity for six-membered acetal is always higher and at lower conversions 100% selectivity for 1,3-dioxane was obtained using 20% MoO_3/SiO_2 catalyst. Corma and co-workers [52] have also reported the acetalization of propylene glycol with methyl napthyl ketone using USY and beta zeolite with different Si/Al ratio at 150 °C and excess of glycol (2.5 equiv.). Very high yields up to 99% were obtained with USY, though slightly lower catalytic activity was observed in case of beta catalysts.

Deutsch et al. [30] have used amberlyst-36 resin, nafion, H-beta and montmorillinite K-10 as catalysts for condensation of glycerol with different benzaldehyde, formaldehyde and acetone. In case of glycerol and benzaldehyde maximum yield obtained for mixture of both the isomers (dioxolane and dioxane) was 94% with the selectivity for dioxane/dioxolane in the range of 64/39 to 48/52. In this report very high selectivity for any particular isomer could not be achieved though very high conversions were attained.

In all the previous reports very high selectivity for either of the isomer could not be achieved, whereas using MoO_3/SiO_2 high selectivity for six-membered acetal was achieved. The suggested mechanism for acetalization of aldehyde using acid involves protonation of carbonyl group which needs Brønsted acidity [30]. In case of MoO_3/SiO_2 the FTIR of adsorbed pyridines for 20% Mo loading shows the presence of Brønsted acidity along with Lewis acidity. This observation is also supported by Raman spectroscopic studies where formation of silicomolybdic acid on the silica surface is observed in presence of moisture.

It is proven fact that 1,3-dioxolane **(2)** is favored kinetically, and isomerizes to the thermodynamically more stable 1,3-dioxane **(1)**. Climent et al. have carried out the kinetic studies for the acetalization of glycerol with phenylacetaldehyde using ZSM-5 and MOR and have achieved maximum selectivity for 1,3-dioxolane [15]. In case of medium pore zeolite such as ZSM-5 or even for a large pore unidirectional zeolite as MOR the products might face a diffusional restriction that will be more severe for the formation of

Table 3
Acetalization of glycerol with various aldehydes.

Sr. no.	Carbonyl compound	Time, h	Conversion, %	Six-membered, %	Five-membered, %
1.	*p-Tert*-butyl benzaldehyde	8	54	62	38
2.	2-Hydroxy, 5-nitro benzaldehyde	8	23	60	40
3.	Anisaldehyde	8	45	99.5	0.5
4.	*o*-Chloro	8	61	72	28
	Benzaldehyde	16	70	70	30
5.	*n*-Heptaldehyde	8	78	62	38
6.	*n*-Butyraldehyde	8	69	66	34
7.	*Trans*-cinnamaldehyde	8	10	100	00
8.	Phenylacetaldehyde	8	56	91	09

Charge: glycerol = 0.11 mol, carbonyl compounds = 0.1 mol, catalyst (20% MoO_3/SiO_2) = 10 wt% of glycerol, reaction temp = 100 °C, solvent = toluene 15 g.

the transition state for converting 1,3-dioxolane to 1,3-dioxane. The ratio of the two isomers might be due to the shape selectivity effects. In case of 20% MoO_3/SiO_2 as catalyst, the reaction could take place inside the large pores of 20% MoO_3/SiO_2 (Table 1, entry 6). Due to the mesoporous nature of the present catalyst the catalytically active acid sites are easily accessible to the reactants and the faster diffusion of the intermediates and the products into the pores of the catalyst, favors the formation of transition state for converting the 1,3-dioxolane **(2)** to 1,3-dioxane (**1**).

4. Conclusion

MoO_3/SiO_2 catalysts prepared by sol–gel techniques were used successfully for acetalization of glycerol with various aldehydes. High conversion up to 78% was obtained for aliphatic aldehydes. Very high selectivity (up to 100%) for six-membered acetal was obtained at lower conversions (10%); however, up to 70% selectivity for six-membered acetal was obtained at 70% conversion for *o*-chloro benzaldehyde. MoO_3/SiO_2 catalysts with 20 mol% Mo loading were found to be most acidic and highly active catalyst in the series. The extensive characterization of the catalysts shows presence of various well dispersed entities like SMA, polymolybdate species or molybdenum oxide nanoparticles depending on the Mo loading. The present sol–gel method of preparation allowed us to increase the dispersion and the range of existence of the Mo entities with the Mo loading. It has been shown that the SMA at low Mo loading was not formed during the sol–gel process but by the rehydration of the calcined catalyst due to the presence of nanosize molybdenum oxospecies supported on high surface mesoporous silica support. This was directly correlated to the ZPC of the silica support, which permits the preservation of this HPA that is only stable in solution at low pH values typically below 2. The increase of the Mo loading induces an increase of the pH of the solution inside the pores and in agreement with literature data, the presence of a well dispersed surface polymolybdate is observed. It has also been shown that the formation of aggregates of α-MoO_3 particles at high Mo loadings originates from the AHM precipitation during the sol–gel preparation. But intermediately β-MoO_3 nanoparticles are stabilized even after calcination at 500 °C. The acidity measurements are in good agreement with this description, well dispersed phases exhibiting only Lewis acidity, whereas molybdenum oxide particles exhibit both Lewis and Brønsted ones.

References

[1] A. Behr, J. Eilting, K. Irawadi, J. Leshinki, F. Lindner, Green Chem. 10 (2008) 13–30.
[2] A.T. Marshall, R.G. Haverkamp, Int. J. Hydrogen Energy 33 (2008) 4649–4654.
[3] J.A. Melero, R.V. Grieken, G. Morales, M. Paniagua, Energy Fuels 21 (2007) 1782–1791.
[4] A. Nemeth, B. Sevella, Appl. Biochem. Biotechnol. 144 (2007) 47–58.
[5] L. Ott, M. Bicker, H. Vogel, Green Chem. 8 (2006) 214–220.
[6] M. Watanabe, Bioresour. Technol. 98 (2007) 1285–1292.
[7] S.S. Yazdani, R. Gonzalez, Curr. Opin. Biotechnol. 18 (2007) 213–219.
[8] J.X. Jiang, P.P. Zhang, C. Yao, Xiandai Huagong/Mod. Chem. Ind. 26 (2006) 71–73.
[9] Chen, ICIS Chem. Business 25 (2007) 1.
[10] T. Werpy, G. Peterson, Top Value Added Chemicals from Biomass, U.S. Department of Energy, Oak Ridge, TN, USA, 2004.
[11] A.J. Showler, P.A. Darley, Chem. Rev. 67 (1967) 427–440.
[12] T.W. Green, P.G.M. Wuts, Protective Groups in Organic Synthesis, vol. 4, 2nd ed., Wiley, New York, 1991, p. 212.
[13] K. Bauer, D. Garbe, H. Surburg, Common Fragrances and Flavours Materials, 2nd ed., VCH, New York, 1990.
[14] D. Ballivet-Tkatchenko, S. Chambrey, R. Keiski, R. Ligabue, L. Plasseraud, P. Richard, H. Turunen, Catal. Today 115 (2006) 80–87.
[15] M.J. Climent, A. Corma, A. Velty, Appl. Catal. A: Gen. 263 (2004) 155–161.
[16] K. Woelfel, T.G. Hartman, ACS Symp. Ser. 705 (1998) 193–194.
[17] A. Cesar, D.S. Ferreira, J.C. Barbe, A. Bertrand, J. Agric. Food Chem. 50 (2002) 2560–2564.
[18] M. Pagliaro, R. Ciriminna, H. Kimura, M. Rossi, C. Della Pina, Angew. Chem. Int. Ed. 46 (2007) 4434–4439.
[19] G. Cherkaev, S.A. Timonin, G.F. Yakovleva, L. Shutikova, A.S. Mikhailova, L.D. Shapiro, SU 1 (1987) 337.
[20] M.J. Ashton, C. Lawrence, J.A. Karlsson, K.A.J. Stuttle, C.G. Newton, B.Y.J. Vacher, S. Webber, M.J. Withnall, J. Med. Chem. 39 (1996) 4888–4896.
[21] T. Vu Moc, P. Maitte, Bull. Soc. Chim. Fr. 9 (1975) 2558–2560.
[22] L. Tong-Shuang, L. Sheng-Hui, L. Ji-Tai, L. Hui-Zhang, J. Chem. Res. Synop. 1 (1997) 286–287.
[23] M. Csiba, J. Cleophax, A. Loupy, J. Malthete, S.D. Gero, Tetrahedron Lett. 34 (1993) 1787–1790.
[24] A. Corma, M.J. Climent, H. García, J. Primo, Appl. Catal. 59 (1990) 333–336.
[25] R. Ballini, G. Bosica, B. Frullanti, R. Maggi, G. Sartori, F. Schroer, Tetrahedron Lett. 39 (1998) 1615–1618.
[26] I. Rodriguez, M.J. Climent, A. Corma, S. Iborra, V. Fornés, J. Catal. 192 (2000) 441–447.
[27] M.J. Climent, A. Corma, A. Velty, M. Susarte, J. Catal. 196 (2000) 345–351.
[28] M.J. Climent, A. Corma, S. Iborra, M.C. Navarro, J. Primo, J. Catal. 161 (1996) 783–789.
[29] Y. Tanaka, N. Sawamura, M. Iwamoto, Tetrahedron Lett. 39 (1998) 9457–9460.
[30] J. Deutsch, A. Martin, H. Lieske, J. Catal. 245 (2007) 428–433.
[31] A. Corma, L.T. Nemeth, M. Renz, S. Valencia, Nature 412 (2001) 423–425.
[32] A. Corma, M. Domine, L.T. Nemeth, S. Valencia, J. Am. Chem. Soc. 124 (2002) 3194–3195.
[33] N. Ohler, A.T. Bell, J. Catal. 231 (2005) 115–130.
[34] S.K. Maurya, M.K. Gurjar, K.M. Malshe, P.T. Patil, M.K. Dongare, E. Kemnitz, Green Chem. 5 (2003) 720–723.
[35] P.T. Patil, K.M. Malshe, S.P. Dagade, M.K. Dongare, Catal. Commun. 4 (2003) 429–434.
[36] A.V. Biradar, S.B. Umbarkar, M.K. Dongare, Appl. Catal. A 285 (2005) 190–195.
[37] X. Ma, J. Gong, S. Wang, N. Gao, D. Wang, X. Yang, F. He, Catal. Commun. 5 (2004) 101–106.
[38] S.B. Umbarkar, A.V. Biradar, S.M. Mathew, K.M. Malshe, P.T. Patil, S.P. Dagde, S.P. Niphadkar, M.K. Dongare, Green Chem. 8 (2006) 488–493.
[39] S.M. Mathew, A.V. Biradar, S.B. Umbarkar, M.K. Dongare, Cat. Commun. 7 (2006) 394–398.
[40] M.K. Dongare, V.V. Bhagwat, C.V. Ramana, M.K. Gurjar, Tetrahedron Lett. 45 (2004) 4759–4762.
[41] A. Kido, H. Iwamoto, N. Azuma, A. Ueno, Catal. Surv. Asia 6 (2002) 45–47.
[42] C. Martin, G. Plazenet, J. Lynch, B. Rebours, E. Payen, Micropor. Mesopor. Mater. 80 (2004) 275–1275.
[43] L. Iebihan, L. Duhamel, C. Mauchausse, E. Payen, J. Grimblot, J. Sol–Gel Sci. Technol. 2 (1994) 837–842.
[44] J.H. Prish, E.M. Carron, R. Van Dreeele, J.A. Goldstone, J. Solid-State Chem. 93 (1991) 13–21.
[45] J. Stencel, Raman Spectroscopy for Catalysis, Van Nostrend Reinhold, New York, 1990, p. 53.
[46] L. Seguin, M. Figlarz, R. Cavagnat, J.C. Lassègues, Spect. Chem. Acta, A 51 (1995) 1323–1328.
[47] E.M. McCarron, J. Chem. Soc., Chem. Commun. (1986) 336–339.
[48] E. Payen, J. Grimblot, J.C. Lerelley, R. Datuier, F. Mauge, Handbook of Vibrational Spectroscopy, p. 4.
[49] J.N. Chalmers, P.R. Griffiths, editor, John Wiley & Sons Ltd., 2001, p. 2036.
[50] R. Deliche, A. Auissi, M.M. Bettahar, S. Launey, M. Fournier, J. Catal. 164 (1996) 16–27.
[51] S.D. Kohler, J.G. Ekerdt, D.S. Kim, I.E. Wachs, Catal. Lett. 16 (1992) 231–239.
[52] M.J. Climent, A. Velty, A. Corma, Green Chem. 4 (2002) 565–569.